Two-dimensional contact mechanics problems involving inhomogeneously elastic solids split into three distinct layers

Article *in* International Journal of Engineering Science · September 2013

DOI: 10.1016/j.ijengsci.2013.05.004

CITATIONS
4

READS
31

2 authors:

S. J. Chidlow
Liverpool John Moores University
15 PUBLICATIONS **44** CITATIONS
SEE PROFILE

M. Teodorescu
University of California, Santa Cruz
57 PUBLICATIONS **464** CITATIONS
SEE PROFILE

Two-dimensional contact mechanics problems involving inhomogeneously elastic solids split into three distinct layers

S. J. Chidlow*, M. Teodorescu†,*[1]

*School of Engineering, Cranfield University, Cranfield, MK43 0AL, UK
†Baskin School of Engineering, University of California at Santa Cruz, CA USA

Abstract

This paper is concerned with an investigation into the two-dimensional frictionless contact problem of an inhomogeneously elastic material under a rigid punch and in particular the induced sub-surface stress fields. The inhomogeneous solid is deemed to comprise three distinct regions which represent a homogeneously elastic coating and substrate joined together by a functionally graded transition layer whose shear modulus depends exponentially on the vertical coordinate. Using the assumption that the effects of the contact pressure die quickly away from the contact region, we formulate closed form solutions for the horizontal and vertical displacements of the solid which are analytic if the contact pressure is known exactly. These solutions are further used to derive a fast and efficient algorithm from which the contact footprint may be computed.

A selection of numerical results are presented using this method and it is found that our model compares well with those of authors in two particular limiting cases. We then investigate the effects of material inhomogeneity and coating thickness on the circular stamp problem and it is found that hard coatings experience much larger contact pressures than soft coatings but act over a smaller area. These effects are exacerbated by decreased interlayer thickness where hard coatings achieve

[1]*Corresponding author's email address : mteodorescu@soe.ucsc.edu*

their maximum pressure and soft coatings achieve their minimum. This has a knock-on effect on the sub-surface stress fields as the maximum principal stress attained within hard coatings when the interlayer is thin is much larger than when the interlayer is thick. This indicates that the maximum principal stress is highly dependent on not only material inhomogeneity but interlayer thickness as well.

1. Introduction

Contact mechanics problems involving inhomogeneous materials have received increasing attention in recent years as our ability to manufacture more complex materials has advanced dramatically. However, the wide variety of assumptions that can be made about systems comprising a coating-substrate has led to the development of a wide variety of models. The earliest such attempts consider the substrate to be rigid and the coating homogeneous (e.g. Hannah (1951)). If the additional assumption is made that the coating is thin, asymptotic solutions may be obtained which allow considerable simplification of the solution (e.g. Jaffar (1989)). These models however are generally far from realistic and are severely limited in their application.

A more accurate assumption is to model the coating and substrate as distinct yet homogeneous layers which are perfectly bonded at their interface. This approach has been taken by several authors such as Ma and Korsunsky (2004) who used Fourier transforms to formulate a pair of integral equations from which the normal and tangential pressure resulting from contact between two dissimilar inhomogenenously elastic bodies or a rigid stamp and an inhomogeneous body can be determined. An alternate model was presented by Teodorescu et al. (2009) who formulated a numerical algorithm to approximate the contact footprint resulting from frictionless contact between

a rigid circular punch and a layered solid. A selection of numerical results were then presented indicating the effects of hard and soft coatings on the sub-surface stress fields.

As the properties of functionally graded materials (FGM) are continuously changing throughout their volume, a better approximation is to assume that the shear modulus of the coating is dependent on either the horizontal or vertical coordinate in some pre-determined way. The most common assumptions take the shear modulus to follow either a power law or exponential variation. Guler and Erdogan (2004) and Guler and Erdogan (2007) assumed that the coating follows an exponential variation and used Fourier transforms to formulate a pair of coupled integral equations from which the contact pressures could be determined. Assuming Coulomb friction, the authors presented a set of results for a flat stamp, circular stamp, triangular stamp and a wedge-shaped stamp. This approach was also taken by Ke and Wang (2006) and Ke and Wang (2007) with the exception that the coating was assumed to be split into an arbitrary number of layers where the shear modulus in each one depends linearly on the depth coordinate. Both sets of authors present results that are in excellent agreement with each other. An extension to the model of Ke and Wang (2006) was presented by Yang and Ke (2008) who considered a coating-graded layer-substrate formulation. The coating and substrate are both assumed homogeneous whilst the graded layer is split into an arbitrary number of layers with piecewise linear shear moduli. The authors considered the frictionless contact of a rigid circular stamp and presented a selection of results that validate their model in two limiting cases.

This paper is concerned with the derivation of a new model to approximate the contact pressure and contact half-width that results from contact between a rigid stamp and an inhomogeneously

elastic solid. The solid is comprised of a homogeneous coating and substrate joined together by a functionally graded transition layer whose shear modulus depends exponentially on the depth coordinate. We invoke the assumptions of Chidlow et al. (2011) that the effects of the applied pressure die quickly away from the contact region in order to represent the horizontal and vertical displacements within the solid using Fourier series. An iterative algorithm is then presented which allows the fast and efficient solution of the contact problem.

The layout of this paper is as follows. In section (2) we formulate the contact problem which is solved in section (3) when the contact pressure is assumed known. These solutions are examined in more detail in section (4) and their limiting behaviour in three different cases considered. The iterative algorithm used to compute the solution to the frictionless contact problem is presented in section (5) and a selection of numerical results are presented in section (6). Finally, our work is summarised in section (7).

2. Formulation of the problem

We consider an inhomogeneously elastic material in a state of plane strain occupying the region $-L \leq x \leq L, -\infty < y \leq 0$ which comprises three distinct regions. The upper layer (region 1) occupies $-h_1 \leq y \leq 0$ and represents a homogeneously elastic coating, the lower layer (region 3) occupies $-\infty < y \leq -h_2$ and represents a homogeneously elastic substrate whilst the interlayer (region 2) occupies $-h_2 \leq y \leq -h_1$ and represents a transitional layer where the material properties progressively morph from that of the coating to that of the substrate. The shear modulus of the solid

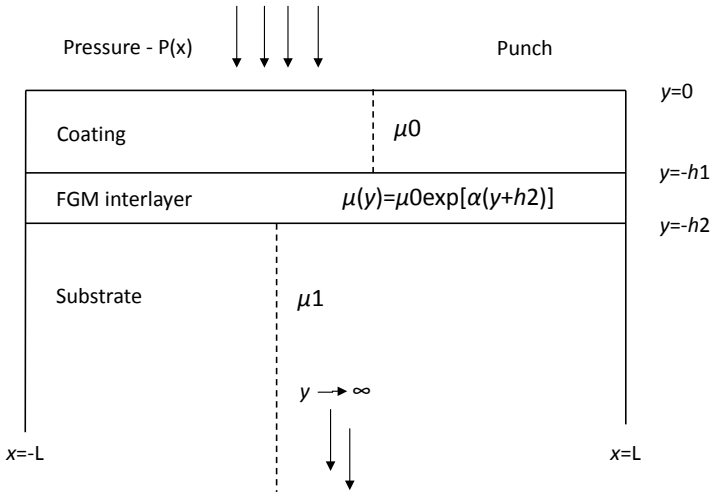

Figure 1: A definition sketch of the problem.

is then defined as

$$\mu(y) = \begin{cases} \mu_1, & -h_1 \leq y \leq 0, \\ \mu_0 e^{\alpha(y+h_2)}, & -h_2 \leq y \leq -h_1, \\ \mu_0, & -\infty < y < -h_2 \end{cases} \tag{1}$$

with

$$\alpha = \frac{1}{h_2 - h_1} \ln\left(\frac{\mu_1}{\mu_0}\right). \tag{2}$$

which ensures that the shear modulus is continuous everywhere. The Poisson ratio within each layer denoted $\nu^{(i)}$, $i = 1,2,3$ is taken to be constant and equivalent and so $\nu^{(1)} = \nu^{(2)} = \nu^{(3)} = \nu$.

Suppose that an external pressure force of the form

$$P(x) = \begin{cases} -p(x), & |x| \leq a, \\ 0, & |x| > a \end{cases} \tag{3}$$

where a denotes the contact half-width is applied normally to the solid surface (see figure (1)). The state of stress at any point within the solid may then be computed by solving the following boundary-value problem (BVP)

$$\frac{2\mu(y)}{1-2\nu}\left((1-\nu)\frac{\partial u}{\partial x}+\nu\frac{\partial v}{\partial y}\right)_x+\left(\mu(y)\left(\frac{\partial u}{\partial y}+\frac{\partial v}{\partial x}\right)\right)_y=0, \qquad -\infty<y\leq 0, \tag{4}$$

$$\mu(y)\left(\frac{\partial u}{\partial y}+\frac{\partial v}{\partial x}\right)_x+\left(\frac{2\mu(y)}{1-2\nu}\left(\nu\frac{\partial u}{\partial x}+(1-\nu)\frac{\partial v}{\partial y}\right)\right)_y=0, \qquad -\infty<y\leq 0, \tag{5}$$

$$\frac{2\mu_1}{1-2\nu}\left(\nu\frac{\partial u}{\partial x}+(1-\nu)\frac{\partial v}{\partial y}\right)-P(x)=0, \qquad (y=0), \tag{6}$$

$$\frac{\partial u}{\partial y}+\frac{\partial v}{\partial x}=0, \qquad (y=0), \tag{7}$$

$$(1-\nu)\frac{\partial u}{\partial x}+\nu\frac{\partial v}{\partial y}=0, \qquad (x=\pm L), \tag{8}$$

$$v=0, \qquad (x=\pm L), \tag{9}$$

$$|u|,|v|\to 0, \qquad (y\to-\infty), \tag{10}$$

subject to the matching conditions

$$u^{(i)}-u^{(i+1)}=0, \qquad (y=-h_i), \tag{11}$$

$$v^{(i)}-v^{(i+1)}=0, \qquad (y=-h_i), \tag{12}$$

$$\left(\nu\frac{\partial u^{(i)}}{\partial x}+(1-\nu)\frac{\partial v^{(i)}}{\partial y}\right)-\left(\nu\frac{\partial u^{(i+1)}}{\partial x}+(1-\nu)\frac{\partial v^{(i+1)}}{\partial y}\right)=0, \qquad (y=-h_i), \tag{13}$$

$$\left(\frac{\partial u^{(i)}}{\partial y}+\frac{\partial v^{(i)}}{\partial x}\right)-\left(\frac{\partial u^{(i+1)}}{\partial y}+\frac{\partial v^{(i+1)}}{\partial x}\right)=0, \qquad (y=-h_i) \tag{14}$$

for $i=1,2$. The surface boundary conditions and matching conditions outlined above represent frictionless contact and ensure that all three layers are perfectly bonded to each other. The radiation conditions $|u|\to 0$, $|v|\to 0$ as $y\to-\infty$ ensures that the solution remains bounded whilst the

boundary conditions at $x = \pm L$ represent the limits at which the applied pressure is hypothesised to cease to effect the solid. The choice of L is discussed in more detail in section (6).

3. Solving the BVP

3.1. Separation solutions

We attempt to solve the BVP outlined above by seeking separation solutions of the form $u(x,y) = A(x)f(y)$, $v(x,y) = B(x)g(y)$ which satisfy the boundary conditions on $x = \pm L$. It is easily verified that

$$u(x,y) = A_0(y) + \sum_{n=1}^{\infty} A_n(y) \cos\left(\frac{1}{2}\beta_n(x+L)\right), \tag{15}$$

$$v(x,y) = \sum_{n=1}^{\infty} B_n(y) \sin\left(\frac{1}{2}\beta_n(x+L)\right) \tag{16}$$

$n \in \ltimes$, $\beta_n = n\pi/L$ satisfy the necessary conditions. As the boundary conditions at $x = \pm L$ are the same within each region, we see that the form of the displacements in the coating, substrate and interlayer are given by (15) and (16). Substituting (15) and (16) into (4) and (5) allows us to determine the functions $A_n(y)$ and $B_n(y)$ in each layer and construct the general solutions

$$u^{(1)}(x,y) = C_0^{(1)} + C_0^{(2)}y + \sum_{n=1}^{\infty} \left((C_n^{(1)} + C_n^{(2)}y)e^{\frac{1}{2}\beta_n y} + (C_n^{(3)} + C_n^{(4)}y)e^{-\frac{1}{2}\beta_n y}\right) \cos\left(\frac{1}{2}\beta_n(x+L)\right), \tag{17}$$

$$v^{(1)}(x,y) = \sum_{n=1}^{\infty} \left((D_n^{(1)} + D_n^{(2)}y)e^{\frac{1}{2}\beta_n y} + (D_n^{(3)} + D_n^{(4)}y)e^{-\frac{1}{2}\beta_n y}\right) \sin\left(\frac{1}{2}\beta_n(x+L)\right) \tag{18}$$

which hold for $-L \le x \le L, -h_1 \le y \le 0$,

$$u^{(2)}(x,y) = A_0^{(1)} + A_0^{(2)} e^{\alpha y} + \sum_{n=1}^{\infty} \left(\sum_{j=1}^{4} A_n^{(j)} e^{\lambda_{j,n} y} \right) \cos\left(\frac{1}{2} \beta_n (x+L) \right), \tag{19}$$

$$v^{(2)}(x,y) = \sum_{n=1}^{\infty} \left(\sum_{j=1}^{4} B_n^{(j)} e^{\lambda_{j,n} y} \right) \sin\left(\frac{1}{2} \beta_n (x+L) \right) \tag{20}$$

where the roots $\lambda_{j,n}$ are defined as

$$\lambda_{1,n} = \sqrt{\frac{1}{4}(\alpha^2 + \beta_n^2) + \frac{i}{2}\alpha\beta_n \sqrt{\frac{\nu}{1-\nu}}} - \frac{1}{2}\alpha, \tag{21}$$

$$\lambda_{2,n} = -\sqrt{\frac{1}{4}(\alpha^2 + \beta_n^2) + \frac{i}{2}\alpha\beta_n \sqrt{\frac{\nu}{1-\nu}}} - \frac{1}{2}\alpha, \tag{22}$$

$$\lambda_{3,n} = \sqrt{\frac{1}{4}(\alpha^2 + \beta_n^2) - \frac{i}{2}\alpha\beta_n \sqrt{\frac{\nu}{1-\nu}}} - \frac{1}{2}\alpha, \tag{23}$$

$$\lambda_{4,n} = -\sqrt{\frac{1}{4}(\alpha^2 + \beta_n^2) - \frac{i}{2}\alpha\beta_n \sqrt{\frac{\nu}{1-\nu}}} - \frac{1}{2}\alpha, \tag{24}$$

which holds for $-L \le x \le L, -h_2 \le x < -h_1$ and

$$u^{(3)}(x,y) = E_0^{(1)} + E_0^{(2)} y + \sum_{n=1}^{\infty} \left((E_n^{(1)} + E_n^{(2)} y) e^{\frac{1}{2}\beta_n y} + (E_n^{(3)} + E_n^{(4)} y) e^{-\frac{1}{2}\beta_n y} \right) \cos\left(\frac{1}{2} \beta_n (x+L) \right), \tag{25}$$

$$v^{(3)}(x,y) = \sum_{n=1}^{\infty} \left((F_n^{(1)} + F_n^{(2)} y) e^{\frac{1}{2}\beta_n y} + (F_n^{(3)} + F_n^{(4)} y) e^{-\frac{1}{2}\beta_n y} \right) \sin\left(\frac{1}{2} \beta_n (x+L) \right) \tag{26}$$

which hold for $-L \leq x \leq L, -\infty < y < -h_2$. The constants appearing above are not independent and are related through the identities

$$D_n^{(1)} = C_n^{(1)} - \delta_n C_n^{(2)}, \qquad D_n^{(2)} = C_n^{(2)}, \tag{27}$$

$$D_n^{(3)} = -(C_n^{(3)} + \delta_n C_n^{(4)}), \qquad D_n^{(4)} = -C_n^{(4)}, \tag{28}$$

$$F_n^{(1)} = E_n^{(1)} - \delta_n E_n^{(2)}, \qquad F_n^{(2)} = E_n^{(2)}, \tag{29}$$

$$F_n^{(3)} = -(E_n^{(3)} + \delta_n E_n^{(4)}), \qquad F_n^{(4)} = -E_n^{(4)}, \tag{30}$$

$$B_n^{(j)} = -\gamma_{j,n} A_n^{(j)}, \tag{31}$$

$n \in \mathbb{N}, j = 1, ..., 4$. The constants δ_n and $\gamma_{j,n}$ are defined as

$$\delta_n = \frac{2(3-4\nu)}{\beta_n}, \tag{32}$$

$$\gamma_{j,n} = \frac{2\left((1-2\nu)\lambda_{j,n}^2 + \alpha(1-2\nu)\lambda_{j,n} - \frac{1}{2}(1-\nu)\beta_n^2\right)}{\beta_n\left(\lambda_{j,n} + \alpha(1-2\nu)\right)}. \tag{33}$$

As the roots $\lambda_{j,n}$ satisfy $\lambda_{3,n} = \bar{\lambda}_{1,n}$, $\lambda_{4,n} = \bar{\lambda}_{2,n}$, it follows that $\gamma_{3,n} = \bar{\gamma}_{1,n}$, $\gamma_{4,n} = \bar{\gamma}_{2,n}$.

3.2. Determination of the final solution

It is only left to determine the constants appearing in (17), (18), (25), (26), (19) and (20) using the remaining boundary and matching conditions. We immediately see that the radiation conditions $|u|, |v| \to 0$ as $y \to -\infty$ can only be satisfied if $E_0^{(1)} = E_0^{(2)} = E_n^{(3)} = E_n^{(4)} = F_n^{(3)} = F_n^{(4)} = 0$. The surface boundary conditions imply the system

$$R_n \begin{pmatrix} C_n^{(1)} \\ C_n^{(2)} \end{pmatrix} + S_n \begin{pmatrix} C_n^{(3)} \\ C_n^{(4)} \end{pmatrix} = -\frac{1}{2\mu_1} \begin{pmatrix} P_n \\ 0 \end{pmatrix}, \tag{34}$$

whilst the interfacial matching conditions at $y=-h_1$ and $y=-h_2$ can be combined to yield the relations

$$\begin{pmatrix} E_n^{(1)} \\ E_n^{(2)} \end{pmatrix} = \frac{e^{\frac{1}{2}\beta_n h_2}}{\delta_n} \left(Z_{1,n}^{(2)} K_{1,n}^{(2)} \begin{pmatrix} A_n^{(1)} \\ A_n^{(3)} \end{pmatrix} + Z_{2,n}^{(2)} K_{2,n}^{(2)} \begin{pmatrix} A_n^{(2)} \\ A_n^{(4)} \end{pmatrix} \right), \tag{35}$$

$$\begin{pmatrix} A_n^{(2)} \\ A_n^{(4)} \end{pmatrix} = -\left(K_{2,n}^{(2)}\right)^{-1} T_{2,n}^{-1} T_{1,n} K_{1,n}^{(2)} \begin{pmatrix} A_n^{(1)} \\ A_n^{(3)} \end{pmatrix} \tag{36}$$

and

$$\begin{pmatrix} C_n^{(1)} \\ C_n^{(2)} \end{pmatrix} = \frac{e^{\frac{1}{2}\beta_n h_2}}{\delta_n} \left(Z_{1,n}^{(1)} K_{1,n}^{(1)} \begin{pmatrix} A_n^{(1)} \\ A_n^{(3)} \end{pmatrix} + Z_{2,n}^{(1)} K_{2,n}^{(1)} \begin{pmatrix} A_n^{(2)} \\ A_n^{(4)} \end{pmatrix} - e^{\frac{1}{2}\beta_n h_1} \Lambda_n \begin{pmatrix} C_n^{(3)} \\ C_n^{(4)} \end{pmatrix} \right), \tag{37}$$

$$\begin{pmatrix} C_n^{(3)} \\ C_n^{(4)} \end{pmatrix} = e^{-\frac{1}{2}\beta_n h_1} J_n^{-1} \left(T_{1,n} K_{1,n}^{(1)} \begin{pmatrix} A_n^{(1)} \\ A_n^{(3)} \end{pmatrix} + T_{2,n} K_{2,n}^{(1)} \begin{pmatrix} A_n^{(2)} \\ A_n^{(4)} \end{pmatrix} \right). \tag{38}$$

respectively. These equations may be readily combined to give the closed form solutions

$$\begin{pmatrix} A_n^{(1)} \\ A_n^{(3)} \end{pmatrix} = -\frac{e^{-\frac{1}{2}\beta_n h_1}}{2\mu_1}\Phi_n^{-1}\begin{pmatrix} P_n \\ 0 \end{pmatrix}, \tag{39a}$$

$$\begin{pmatrix} A_n^{(2)} \\ A_n^{(4)} \end{pmatrix} = \frac{e^{-\frac{1}{2}\beta_n h_1}}{2\mu_1}\left(T_{2,n}K_{2,n}^{(2)}\right)^{-1}T_{1,n}K_{1,n}^{(2)}\Phi_n^{-1}\begin{pmatrix} P_n \\ 0 \end{pmatrix}, \tag{39b}$$

$$\begin{pmatrix} C_n^{(1)} \\ C_n^{(2)} \end{pmatrix} = -\frac{1}{2\mu_1\delta_n}\Big(Z_{1,n}^{(1)}K_{1,n}^{(1)} - \Delta_n J_n^{-1}W_n$$

$$- Z_{2,n}^{(1)}K_{2,n}^{(1)}\left(T_{2,n}K_{2,n}^{(2)}\right)^{-1}T_{1,n}K_{1,n}^{(2)}\Big)\Phi_n^{-1}\begin{pmatrix} P_n \\ 0 \end{pmatrix}, \tag{39c}$$

$$\begin{pmatrix} C_n^{(3)} \\ C_n^{(4)} \end{pmatrix} = -\frac{e^{-\beta_n h_1}}{2\mu_1}J_n^{-1}W_n\Phi_n^{-1}\begin{pmatrix} P_n \\ 0 \end{pmatrix}, \tag{39d}$$

$$\begin{pmatrix} E_n^{(1)} \\ E_n^{(2)} \end{pmatrix} = -\frac{1}{2\mu_1\delta_n}\left(Z_{1,n}K_{1,n}^{(2)} - Z_{2,n}T_{2,n}^{-1}T_{1,n}K_{1,n}^{(2)}\right)\Phi_n^{-1}\begin{pmatrix} P_n \\ 0 \end{pmatrix}. \tag{39e}$$

together with $C_0^{(1)} = C_0^{(2)} = A_0^{(1)} = A_0^{(2)} = 0$. The quantities P_n, $n \in \mathbb{N}$ appearing above are the coefficients in the Fourier series representation of the pressure and are defined as

$$\begin{aligned} P_n &= \frac{1}{L}\int_{-L}^{L} P(x)\sin\left(\frac{1}{2}\beta_n(x+L)\right), \\ &= -\frac{1}{L}\int_{-a}^{a} p(x)\sin\left(\frac{1}{2}\beta_n(x+L)\right). \end{aligned} \tag{40}$$

These constants are by far the most important quantities that appear in the solution as they provide a direct link between the applied surface pressure and the induced stresses and displacement. The remaining quantities appearing in (39a)-(39e) are all 2×2 matrices which are given explicitly in

the appendix.

4. Limiting cases

Under certain conditions, we can considerably simplify the solutions u and v appearing above. We consider three particular examples here in order to confirm that our model reduces correctly in these limits.

4.1. Case 1: Infinitely thick transition region

We initially consider the case $h_2 \to \infty$ which corresponds to removing the substrate from the problem. Examination of the roots $\lambda_{j,n}$, $j = 1,..,4$ reveals that $\mathrm{Re}(\lambda_{1,n}) > 0, \mathrm{Re}(\lambda_{2,n}) < 0$ and so

$$K_{1,n}^{(2)} \to 0$$

$$(K_{2,n}^{(2)})^{-1} \to 0$$

as $h_2 \to \infty$. We can now deduce that

$$W_n \to T_{1,n} K_{1,n}^{(1)},$$

$$\Phi_n \to \left(\frac{1}{\delta_n} R_n \left(Z_{1,n}^{(1)} - \Lambda_n J_n^{-1} T_{1,n} \right) + e^{-\beta_n h_1} S_n J_n^{-1} T_{1,n} \right) K_{1,n}^{(1)}$$

and so

$$\begin{pmatrix} A_n^{(1)} \\ A_n^{(3)} \end{pmatrix} \to -\frac{e^{-\frac{1}{2}\beta_n h_1}}{2\mu_1}(K_{1,n}^{(1)})^{-1}\left(\frac{1}{\delta_n}R_n\left(Z_{1,n}^{(1)}-\Lambda_n J_n^{-1}T_{1,n}\right)+e^{-\beta_n h_1}S_n J_n^{-1}T_{1,n}\right)\begin{pmatrix} P_n \\ 0 \end{pmatrix},$$

$$\begin{pmatrix} A_n^{(2)} \\ A_n^{(4)} \end{pmatrix} \to 0,$$

$$\begin{pmatrix} C_n^{(1)} \\ C_n^{(2)} \end{pmatrix} \to \frac{1}{\delta_n}\left(Z_{1,n}^{(1)}K_{1,n}^{(1)}-\Lambda_n J_n^{-1}T_{1,n}K_{1,n}^{(1)}\right)\Phi_n^{-1}\begin{pmatrix} A_n^{(1)} \\ A_n^{(2)} \end{pmatrix},$$

$$\begin{pmatrix} C_n^{(3)} \\ C_n^{(4)} \end{pmatrix} \to e^{-\frac{1}{2}\beta_n h_1}J_n^{-1}T_{1,n}K_{1,n}^{(1)}\begin{pmatrix} A_n^{(1)} \\ A_n^{(3)} \end{pmatrix}$$

as $h_2 \to \infty$. It is easily verified that the expressions obtained for the constants here are equivalent to those obtained for the problem of a finitely thick homogeneously elastic coating bonded to an infinitely thick FGM.

4.2. Case 2: Removal of the coating

We now consider what happens to our solution if $h_1 = 0$. An immediate consequence of this assumption is that $K_{j,n}^{(1)}$, $j = 1,2$ reduce to the 2×2 identity matrices. Using this information and

setting $h_1 = 0$ in the matrices appearing in (39a)-(39e)

$$W_n = T_{1,n} - T_{2,n}\left(T_{2,n}K_{2,n}^{(2)}\right)^{-1} T_{1,n}K_{1,n}^{(2)},$$

$$\Phi_n = \frac{1}{\delta_n}R_n Z_{1,n}^{(1)} + \frac{1}{1-2\nu}\begin{pmatrix} 1 & 0 \\ 0 & 1-2\nu \end{pmatrix} T_{1,n}$$

$$- \left(\frac{1}{\delta_n}R_n Z_{2,n}^{(1)} + \frac{1}{1-2\nu}\begin{pmatrix} 1 & 0 \\ 0 & 1-2\nu \end{pmatrix} T_{2,n}\right)\left(T_{2,n}K_{2,n}^{(2)}\right)^{-1} T_{1,n}K_{1,n}^{(2)}.$$

The expression for Φ_n may be further simplified to give

$$\Phi_n = \frac{1}{1-2\nu}\begin{pmatrix} 1 & 0 \\ 0 & 1-2\nu \end{pmatrix}\left(N_{1,n} - N_{2,n}\left(T_{2,n}K_{2,n}^{(2)}\right)^{-1} T_{1,n}K_{1,n}^{(2)}\right)$$

which when used in conjunction with (39a) yields

$$\begin{pmatrix} A_n^{(1)} \\ A_n^{(3)} \end{pmatrix} = -\frac{1}{2\mu_1}\left(N_{1,n} - N_{2,n}\left(T_{2,n}K_{2,n}^{(2)}\right)^{-1} T_{1,n}K_{1,n}^{(2)}\right)^{-1}\begin{pmatrix} P_n \\ 0 \end{pmatrix}.$$

Comparing these results with those of Chidlow et al. (2011) verifies that this solution corresponds to that for a finitely thick functionally graded coating bonded to an infinitely thick substrate. We may therefore conclude that the model derived in this work reduces to the correct limit as $h_1 \to 0$.

4.3. Infinitesimally thin interlayer

Suppose that the thickness of the graded interlayer is negligible so that $(h_2 - h_1)/a \ll 1$. By considering (2), we see that this limit implies that

$$\frac{1}{|\alpha|} = \varepsilon \to 0$$

which we can use as the basis for an asymptotic analysis into the behaviour of our solution in this case. Assuming that $1/\alpha = \varepsilon$ is a very small parameter in (21) allows us to expand the square root in a Taylor series and determine that

$$\lambda_{1,n} = \frac{1}{2}\beta_n \left(i\sqrt{\rho} + \frac{\beta_n \varepsilon}{2(1-\nu)} \right) + \mathrm{O}\left(\varepsilon^2\right), \tag{41}$$

$$\lambda_{2,n} = -\frac{1}{2}\left(\frac{2}{\varepsilon} + i\sqrt{\rho}\beta_n + \frac{\beta_n^2 \varepsilon}{2(1-\nu)} \right) + \mathrm{O}\left(\varepsilon^2\right) \tag{42}$$

and consequentially from (31)

$$\gamma_{1,n} = \frac{1}{2(1-\nu)} \left(2i(1-\nu)\sqrt{\rho} - \beta_n \varepsilon \right), \tag{43}$$

$$\gamma_{2,n} = -\frac{1}{8\nu(1-\nu)} \left(4(1-2\nu)(1-\nu) i\sqrt{\rho} - \beta_n \varepsilon \right). \tag{44}$$

These expressions may be substituted into the matrices appearing in (39a)-(39e) and they allow us to deduce that

$$Z_{2,n}^{(1)} K_{2,n}^{(1)} (T_{2,n} K_{2,n}^{(2)})^{-1} T_{1,n} K_{1,n}^{(2)} = \mathrm{O}(\varepsilon),$$

so at leading order

$$\Phi_n = \frac{1}{\delta_n} R_n \left(Z_{1,n}^{(1)} K_{1,n}^{(1)} - \Lambda_n J_n^{-1} W_n \right) + e^{-\beta_n h_1} S_n J_n^{-1} W_n.$$

In this situation, the constants $C_n^{(1)}$ and $C_n^{(2)}$ may be computed from the formula

$$\begin{aligned}
\begin{pmatrix} C_n^{(1)} \\ C_n^{(2)} \end{pmatrix} &= -\frac{1}{2\mu_1\delta_n}\left(Z_{1,n}^{(1)}K_{1,n}^{(1)} - \Lambda_n J_n^{-1}W_n\right)\left(\frac{1}{\delta_n}R_n\left(Z_{1,n}^{(1)}K_{1,n}^{(1)} - \Lambda_n J_n^{-1}W_n\right)\right. \\
&\qquad \left. + e^{-\beta_n h_1}S_n J_n^{-1}W_n\right)^{-1}\begin{pmatrix} P_n \\ 0 \end{pmatrix}, \\
&= -\frac{1}{2\mu_1\delta_n}\left(\frac{1}{\delta_n}R_n + e^{-\beta_n h_1}S_n\Psi_n^{-1}\right)^{-1}\begin{pmatrix} P_n \\ 0 \end{pmatrix}, \\
&= -\frac{1}{2\mu_1}\left(R_n + \delta_n e^{-\beta_n h_1}S_n\Psi_n^{-1}\right)^{-1}\begin{pmatrix} P_n \\ 0 \end{pmatrix}
\end{aligned}$$

where

$$\Psi_n = Z_{1,n}^{(1)}K_{1,n}^{(1)}W_n^{-1}J_n - \Lambda_n.$$

Further use of (41) and (43) yields

$$\begin{aligned}
Z_{1,n}^{(1)} &= \begin{pmatrix} h_1(1+i\sqrt{\rho}) + \delta_n & h_1(1-i\sqrt{\rho}) + \delta_n \\ 1+i\sqrt{\rho} & 1-i\sqrt{\rho} \end{pmatrix} + \mathrm{O}(\varepsilon), \\
K_{1,n}^{(1)} &= \begin{pmatrix} e^{-\frac{i}{2}\beta_n\sqrt{\rho}h_1} & 0 \\ 0 & e^{\frac{i}{2}\beta_n\sqrt{\rho}h_1} \end{pmatrix} + \mathrm{O}(\varepsilon), \\
W_n &= \begin{pmatrix} \frac{1}{2}(1-2\nu)\big((1-2\nu) - 2i(1-\nu)\sqrt{\rho}\big) & \frac{1}{2}(1-2\nu)\big((1-2\nu) + 2i(1-\nu)\sqrt{\rho}\big) \\ 2(1-\nu) - i(1-2\nu)\sqrt{\rho} & 2(1-\nu) + i(1-2\nu)\sqrt{\rho} \end{pmatrix} \\
&\quad \times \frac{\beta_n}{3-4\nu}\left(\frac{\mu_0}{\mu_1} - 1\right)\begin{pmatrix} e^{-\frac{i}{2}\beta_n\sqrt{\rho}h_1} & 0 \\ 0 & e^{\frac{i}{2}\beta_n\sqrt{\rho}h_1} \end{pmatrix} + \mathrm{O}(\varepsilon),
\end{aligned}$$

so that

$$\Psi_n = \frac{1}{\left(\frac{\mu_0}{\mu_1}-1\right)}\times$$
$$\begin{pmatrix} -(2h_1+\delta_n)\left(\frac{\mu_0}{\mu_1}+(3-4\nu)\right) & \frac{2}{\beta_n}\left(h_1^2\beta_n\frac{\mu_0}{\mu_1}+(3-4\nu)\beta_n h_1^2-4(1-\nu)(1-2\nu)\delta_n\right) \\ -2\left(\frac{\mu_0}{\mu_1}+(3-4\nu)\right) & (2h_1-\delta_n)\left(\frac{\mu_0}{\mu_1}+(3-4\nu)\right) \end{pmatrix}$$

and thus

$$\Psi_n^{-1} = \frac{\beta_n\left(\frac{\mu_0}{\mu_1}-1\right)}{2\delta_n\left(\frac{\mu_0}{\mu_1}+(3-4\nu)\right)\left((3-4\nu)\frac{\mu_0}{\mu_1}+1\right)}\times$$
$$\begin{pmatrix} (2h_1-\delta_n)\left(\frac{\mu_0}{\mu_1}+(3-4\nu)\right) & -\frac{2}{\beta_n}\left(h_1^2\beta_n\frac{\mu_0}{\mu_1}+(3-4\nu)\beta_n h_1^2-4(1-\nu)(1-2\nu)\delta_n\right) \\ 2\left(\frac{\mu_0}{\mu_1}+(3-4\nu)\right) & -(2h_1+\delta_n)\left(\frac{\mu_0}{\mu_1}+(3-4\nu)\right) \end{pmatrix}+\mathrm{O}(\varepsilon).$$

Comparing this result with the solution presented in the appendix (B.19) for a solid comprising two perfectly bonded homogeneous layers, we see that

$$\delta_n\Psi_n^{-1} = \left(1-\frac{\mu_1}{\mu_0}\right)\left(\frac{\mu_1}{\mu_0}S_n^{(1)}-R_n^{(1)}G_n^{-1}H_n\right)^{-1}R_n^{(1)}. \tag{45}$$

We can therefore deduce that as $h_2-h_1\to 0$, the derived model for the full three-layer problem reduces to that of a solid comprising two distinct yet homogeneous layers.

It has been verified in the three limiting cases outlined above that our model behaves like the corresponding two-layer models that describe these simpler problems. We now turn our attention to determining approximations to the surface pressure $p(x)$ for a certain class of contact problems.

5. Contact by a rigid stamp

In the previous section, we derived the solution of the horizontal and vertical displacements within each region that result from the application of a known pressure force to the surface of the

FGM. We now show how we may use these solutions to determine the solution of the frictionless stamp problem.

5.1. Integral equation formulation

We note from (18) that the vertical displacement of the solid surface may be written as

$$\hat{v}(x) = v(x,0) = \sum_{n=1}^{\infty} J_n P_n \phi_n(x) \tag{46}$$

where J_n and $\phi_n(x)$ are easily inferred from (39c) and (39d). Differentiating this expression with respect to x gives

$$\hat{v}^{'}(x) = \frac{\partial v}{\partial x}(x,0) = \sum_{n=1}^{\infty} J_n P_n \phi_n^{'}(x). \tag{47}$$

As the stamp profile is given as part of the problem, the exact form of the surface displacement is prescribed and subsequently, the only unknowns present in (47) are the Fourier coefficients P_n. Replacing all coefficients P_n, $n \in \mathbb{N}, n \neq m$ in 47) using (40) gives

$$\hat{v}^{'}(x) = J_m P_m \phi_m^{'}(x) - \frac{1}{L} \int_{-a}^{a} \sum_{\substack{n=1 \\ n \neq m}}^{\infty} J_n \phi_n^{'}(x) \phi_n(t) p(t) \mathrm{d}t. \tag{48}$$

which is a first-kind integral equation of Fredholm type. As this equation is regular, it may be solved using Galerkin's method (see Porter and Stirling (1990) for example) which involves consideration of the weak form of (48). This may be attained by multiplying (48) by the test functions $\chi_j(x)$, $j = 1, ..., M$ and integrating over the contact region, a process which yields

$$(\hat{v}^{'}, \chi_j) = J_m P_m (\phi_m^{'}, \chi_j) - \frac{1}{L} (\mathscr{L} p, \chi_j) \tag{49}$$

with

$$(\mathscr{L}p)(x) = \int_{-a}^{a} \sum_{\substack{n=1 \\ n\neq m}}^{\infty} J_n \phi_n^{'}(x)\phi_n(t)p(t)\mathrm{d}t, \tag{50}$$

$$(f,g) = \int_{-a}^{a} f(x)g(x)\mathrm{d}x. \tag{51}$$

for arbitrary functions $f(x)$ and $g(x)$. The principal advantage of using Galerkin's method is that it will provide highly accurate approximations to inner product quantities involving the contact pressure $p(x)$ even if the approximation to $p(x)$ itself is poor. We therefore concentrate our attention on the estimation of the Fourier coefficients P_n, $n \in \mathbb{N}$ and formulate an approximation to $p(x)$ using its Fourier series rather than directly estimating $p(x)$ itself. With this is mind, we introduce the approximation

$$p(x) = \sum_{i=1}^{M} b_i \chi_i(x) \tag{52}$$

and substitute this into (49) which gives

$$(\hat{v}^{'}, \chi_j) = J_m P_m (\phi_m^{'}, \chi_j) - \frac{1}{L}\sum_{i=1}^{M} b_i (\mathscr{L}\chi_i, \chi_j) \tag{53}$$

for $j = 1, ..., M$. The M equations given by (53) can be written as the system

$$F = J_m P_m \Omega_m - \frac{1}{L}{\tau_m}^T b \tag{54}$$

with

$$b = \left(b_1, b_2, ..., b_M\right)^T, \tag{55}$$

$$F = \left((\hat{v}^{'}, \chi_1), (\hat{v}^{'}, \chi_2), ..., (\hat{v}^{'}, \chi_M)\right)^T, \tag{56}$$

$$\Omega_m = \left((\phi_n^{'}, \chi_1), (\phi_n^{'}, \chi_2), ..., (\phi_n^{'}, \chi_M)\right)^T \tag{57}$$

and $\tau_{ij} = (\mathscr{L}\chi_i, \chi_j)$ for $i, j = 1, ..., M$. As P_m is unknown, (54) comprises $M+1$ unknowns in M equations. We note however that we can obtain an extra equation by substituting (52) into (40) which gives

$$P_m = -\frac{1}{L}(\phi_m, p), \tag{58}$$

$$\approx -\frac{1}{L}\left(\phi_m, \sum_{i=1}^{N} b_i \chi_i\right) = -\frac{1}{L}\sum_{i=1}^{N} b_i(\phi_m, \chi_i) = -\frac{1}{L}{\Theta_m}^T b \tag{59}$$

where

$$\Theta_m = \Big((\phi_n, \chi_1), (\phi_n, \chi_2), ..., (\phi_n, \chi_M)\Big)^T. \tag{60}$$

Re-arranging (54) for b and combining the result with (60) gives the result

$$P_m = \frac{\Theta_m^T {\tau_m}^{-T} F}{1 + J_m {\Theta_m}^T {\tau_m}^{-T} \Omega_m} \tag{61}$$

which holds for $m \in \mathbb{N}$. We can use (61) to determine an approximation to the coefficients of all required Fourier modes and thus we can approximate the pressure induced through contact as well as the sub-surface stress field within the solid.

A good choice of trial function will seek to mimic the behaviour of the unknown pressure function. As this behaviour is dependent on the type of stamp used in the contact problem, a different set of trial functions will need to be used in each problem to optimise the accuracy and efficiency of the approximation. As the examples presented in section (6) consider contact by a circular stamp, we take

$$\chi_j(x) = \sin\left(\frac{j\pi(x+a)}{2a}\right) \tag{62}$$

$j = 1, ..., M$ as it is known that the contact pressure will satisfy $p(-a) = p(a) = 0$.

5.2. Computing the contact half-width

The full solution of the contact problem requires the determination of the contact pressure $p(x)$ and the contact half-width a. We outline an efficient algorithm below that allows the computation of this parameter when the applied load (W) is known.

The total load applied to the FGM is defined as

$$\begin{aligned} W &= -\int_{-L}^{L} P(x)\mathrm{d}x, \\ &= \int_{-a}^{a} p(x)\mathrm{d}x \end{aligned} \tag{63}$$

which can be expressed in terms of a Fourier series as

$$\begin{aligned} W &= -\sum_{n=1}^{\infty} P_n \int_{-a}^{a} \sin\left(\frac{1}{2}\beta_n(x+L)\right), \\ &= 4\sum_{n=1}^{\infty} \frac{(-1)^n P_{2n-1}}{\beta_{2n-1}} \sin\left(\frac{1}{2}a\beta_{2n-1}\right). \end{aligned} \tag{64}$$

By defining the function $f(a)$ for $a > 0$ as

$$f(a) = W - 4\sum_{n=1}^{\infty} \frac{(-1)^n P_{2n-1}}{\beta_{2n-1}} \sin\left(\frac{1}{2}a\beta_{2n-1}\right), \tag{65}$$

we can solve $f(a) = 0$ using iterative techniques as we know that the zero of this function will be the contact half-width. The choice is made here to use the secant method so that each subsequent approximation to a is computed using the formula

$$a_{m+1} = a_m - \frac{\delta f(a_m)}{f(a_m+\varepsilon) - f(a_m)} \tag{66}$$

for $m = 0, 1, ...$ with the initial guess denoted a_0 and $\delta > 0$. As the value of a is typically very small in magnitude, a direct estimate of the error between successive updates a_m and a_{m+1} could

be potentially misleading and so we deem that the true value of a has been found when

$$\frac{|a_{m+1} - a_m|}{a_{m+1}} < 1 \times 10^{-6} \tag{67}$$

which ensures that the approximation to a is highly accurate. We investigate the accuracy of this approximation in the next section.

6. Numerical Results

6.1. Practical considerations

In this section, we present a selection of numerical results that compare the performance of our model with those of other authors and investigate the effects of coating hardness and coating and interlayer thickness on the solution of the contact problem. There are however some practical considerations that need to be taken into account when using our model which we discuss first.

We initially note that the infinite summations that appear in (17), (18), (25), (26), (19) and (20) cannot be used in practise and must be truncated at some finite value N. The value of N used in each example will be stated explicitly.

In the examples considered in this section, we occasionally refer to the case $\mu_1/\mu_0 = 1$. We cannot let $\mu_1/\mu_0 = 1$ exactly as we need to obtain four linearly independent roots of (21). We therefore use the value $\mu_1/\mu_0 = 1.00001$ to produce results for the homogeneously elastic case.

The most important aspect of using this model is determining an appropriate value of L. The value of L represents the horizontal limit at which the effects of the contact pressure are hypothesised to cease to effect the solid. Taking $L \to \infty$ will ensure high accuracy of our solution but it will also be very expensive computationally as we will have to sum a very large number of wave

modes and thus take. Conversely, if we take L to be much smaller, we will need to sum a relatively small number of Fourier modes but we run the risk of neglecting information because the pressure will still have an effect on the solid outside of our chosen interval. Clearly the choice of L is highly important as it requires a compromise between computational efficiency and accuracy.

Chidlow et al. (2011) showed that the choice $L = 10a$ in the case of a two-layer solid comprising a graded elastic coating and homogeneous substrate is a good compromise between computational efficiency and accuracy. We therefore take $L = 10a$ in this work as it is found to be a good choice here. This statement is borne out by the results presented in sections (6.2) and (6.3).

6.2. Example 1: Model validation with the coating removed

It was shown in section (4) that if h_1 is identically zero, the three-layer model proposed here reduces to the two-layer model described in Chidlow et al. (2011). We now wish to compare how the model derived here compares with that derived by Guler and Erdogan (2007) by attempting to replicate one of their examples.

Consider indenting the surface of the solid given in (1) by a rigid cylindrical punch. The parameter values used in this example are $\nu = 0.3$, $a/R = 0.005$, $h/a = 2$ and we take $\mu_1/\mu_0 = 1/7, 1, 7$. The dimensionless stress distributions σ_{yy}/μ_1 and σ_{xx}/μ_1 are presented in figure (2). These results show excellent agreement with those of Guler and Erdogan (2007) (see their figure (18)).

6.3. Example 2: Model validation for a thin interlayer

We endeavour to replicate the results of Ma and Korsunsky (2004) who considered the application of a rigid cylindrical punch to the surface of an inhomogeneously elastic solid comprising

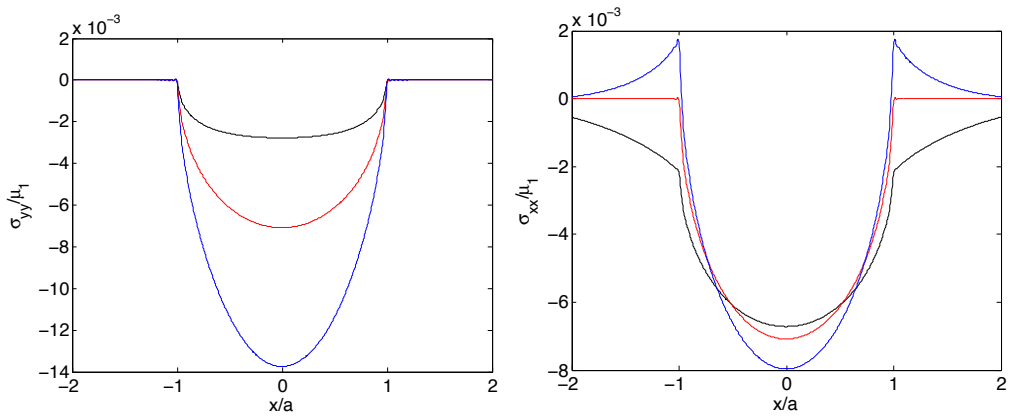

Figure 2: Plots of a) σ_{yy}/μ_1 and b) σ_{xx}/μ_1 produced in example 1 for three different coatings. The blue line shows the soft coating $\mu_1/\mu_0 = 1/7$, the red line the 'homogeneous' coating with $\mu_1/\mu_0 = 1.0001$ and the black line represents the hard coating $\mu_1/\mu_0 = 7$.

two distinct yet homogeneous layers. The parameter values used in this problem are

$$\nu = 0.33, \qquad R = 5 \times 10^{-3} m, \qquad W = 15000N,$$

$$h_1 = 2 \times 10^{-5} m, \qquad E_0 = 1.15 \times 10^{11} \text{Pa}$$

whilst $\mu_1/\mu_0 = 0.5, 1$. In order to accurately reproduce these results, we take $h_2 - h_1 = 1 \times 10^{-7} m$ which ensures that the interlayer is very small in comparison to the coating thickness. The results produced for this problem are presented in figure (3). They show good agreement with those of Ma and Korsunsky (compare with their figure 3)). We obtain the values $a = 33.26\mu$m for the case $\mu_1/\mu_0 = 0.5$ and $a = 27.40\mu$m for the case $\mu_1/\mu_0 = 1$ whilst Ma and Korsunsky obtain $a = 33.10\mu$ m and $a = 27.20\mu$m respectively. This indicates that the residual error between results is less than 1% in both cases.

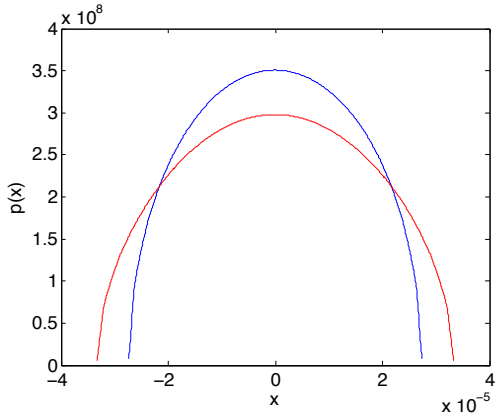

Figure 3: Plots of the pressure p(x) produced in example (6.3). The blue line shows $\mu_1/\mu_0 = 1$ whilst the red line shows $\mu_1/\mu_0 = 0.5$.

6.4. Example 3: The effects of coating thickness and varying load

We now consider an example that allows us to determine the effects that coating and interlayer thickness have on the contact half-width and applied pressure induced by contact with a rigid cylindrical punch. The parameter values used in this problem are $E_0 = 1.15 \times 10^{11}$Pa, $R = 5$cm, $W = 200$N and $\nu = 0.3$.

We will mainly be considering the dimensionless contact half-width $\bar{a} = a/a_h$ and dimensionless pressure $\bar{p}(x) = p(x)/p_h$ within this example as they will allow us to compare our results with those of Hertz and see how the inhomogeneity of the FGM affects the contact problem. The equations used to compute the predicted hertzian contact half-width and maximum contact pressure are included below for brevity.

$$a_h = \sqrt{\frac{2WR(1-\nu)}{\pi\mu_1}}, \qquad p_h = \frac{2W}{\pi a_h} \tag{68}$$

We produce results for five different coatings here satisfying $\mu_1/\mu_0 = 0.25, 0.5, 1, 2$ and 4 subject to the three different relative layer thicknesses $h_1/a_h = 0.1, 0.5, 0.9$. The dimensionless

pressure curves produced for this problem are presented in figure (4) whilst the corresponding subsurface stress fields are presented in figures (5), (6) and (7).

We initially note in figure (4) that the predicted contact half-widths for the soft coatings ($\mu_1/\mu_0 < 1$) increase as the coating thickness increases whilst those predicted for the hard coatings ($\mu_1/\mu_0 > 1$) decrease. The opposite is true however for the maximum contact pressure which increases as the coating thickness increases for the hard coatings and decreases for the soft coatings. These trends were also observed in Chi for a solid comprising a graded-elastic coating and homogeneous substrate. It is additionally observed that the predicted values of a and $p_{\max}$ diverge from the results of Hertz by an increasing margin as the ratio $h_1/a_h \to 1$. This indicates that the innate inhomogeneity of the material under study affects the parameters in the contact problem by an increasing margin as the interlayer shrinks and thus creates a sharper change in the material properties from coating to substrate.

A further interesting feature that can be observed in this example is that an increase in coating thickness coupled with a decrease in interlayer thickness exacerbates the trends described above. We note that the maximum dimensionless contact pressure observed for the hard coating $\mu_1/\mu_0 = 4$ is approximately 1.3 when $h_1/a_h = 0.1$, 1.5 when $h_1/a_h = 0.5$ and 1.7 when $h_1/a_h = 0.9$ whilst it is 0.8, 0.7 and 0.6 respectively for the soft coating $\mu_1/\mu_0 = 0.25$. This suggests that as the interlayer shrinks and we tend to the case of two perfectly bonded distinct homogeneous layers, the contact pressure will attain its maximum for a hard coating and minimum for a soft coating.

We can investigate this behaviour more closely by considering how the contact half-width and maximum pressure changes as the ratio h_1/h_2 changes. The load is is taken to be 200N

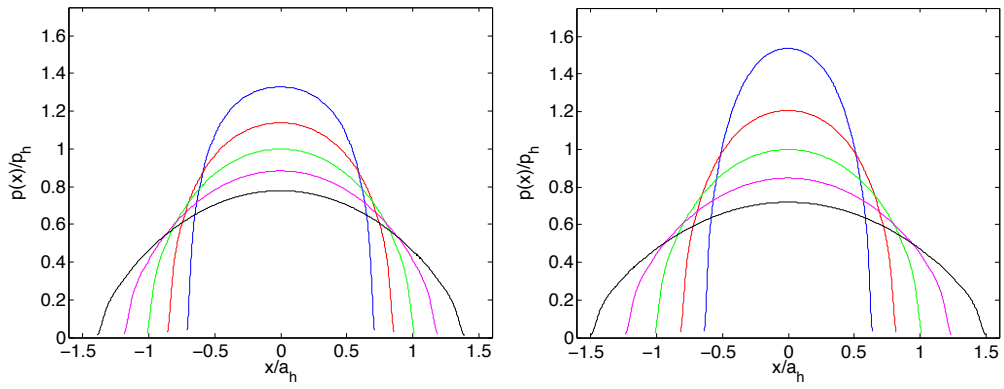

(a) $h_1/a_h = 0.1$ (b) $h_1/a_h = 0.5$

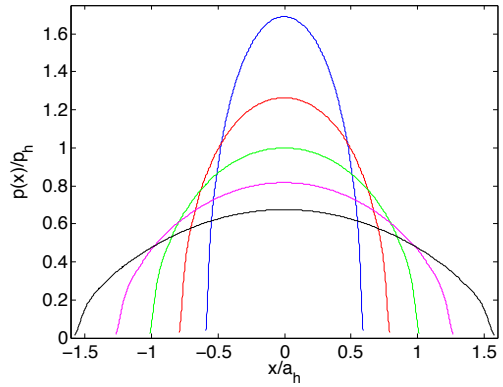

(c) $h_1/a_h = 0.9$

Figure 4: Plots of the dimensionless pressure curves $p(x)/p_h$ produced in example (6.4) for the three different coating thicknesses shown. The blue line depicts $\mu_1/\mu_0 = 4$, the red line $\mu_1/\mu_0 = 2$, the green line $\mu_1/\mu_0 = 1$, the magenta line $\mu_1/\mu_0 = 0.25$ and the black line $\mu_1/\mu_0 = 0.25$.

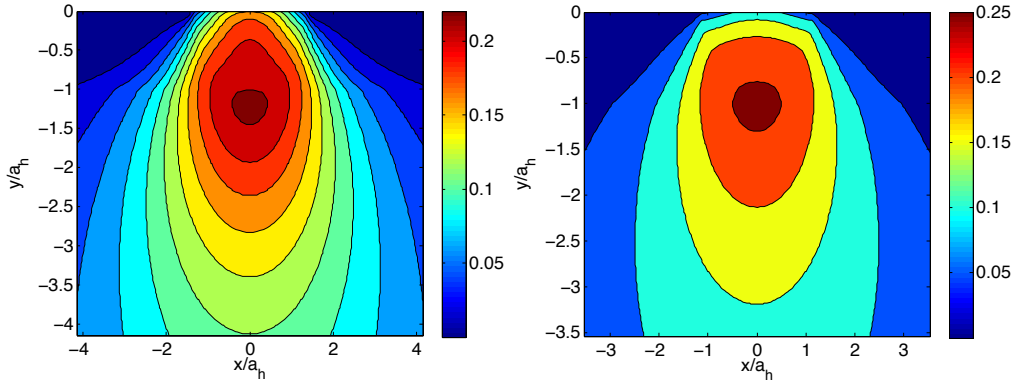

(a) $\mu_1/\mu_0 = 0.25$ (b) $\mu_1/\mu_0 = 0.5$

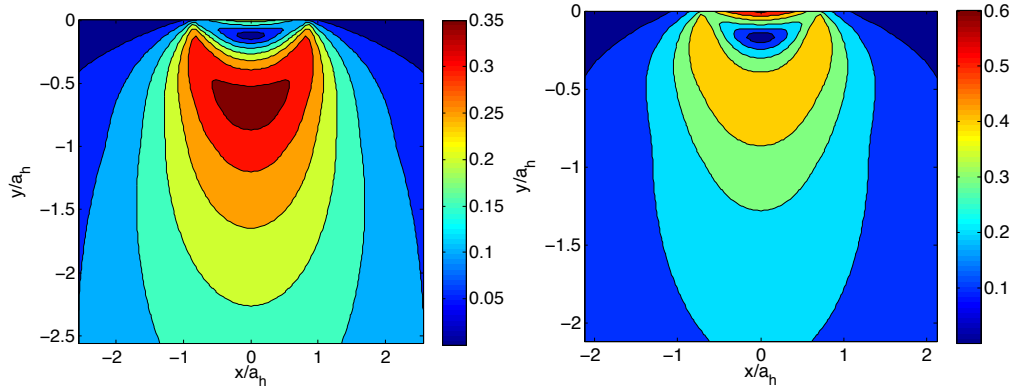

(c) $\mu_1/\mu_0 = 2$ (d) $\mu_1/\mu_0 = 4$

Figure 5: Plots of the dimensionless stress fields τ_1/P_{hertz} for the coatings given above. This set of results corresponds to the thin coating $h/a_h = 0.1$.

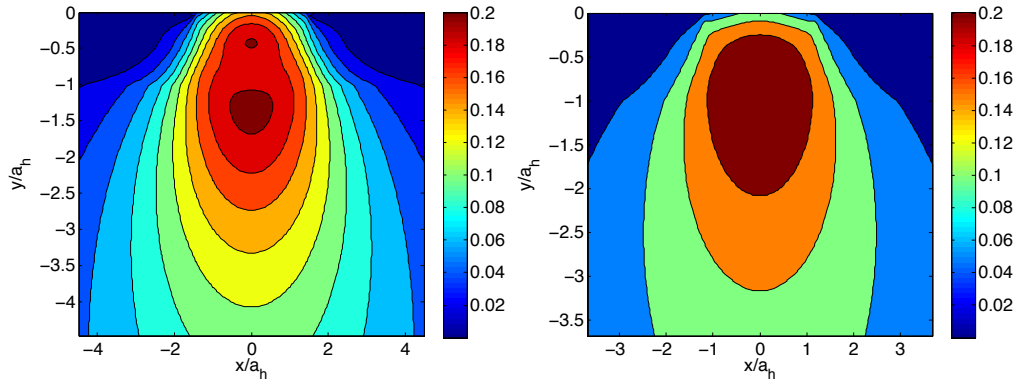

(a) $\mu_1/\mu_0 = 0.25$ (b) $\mu_1/\mu_0 = 0.5$

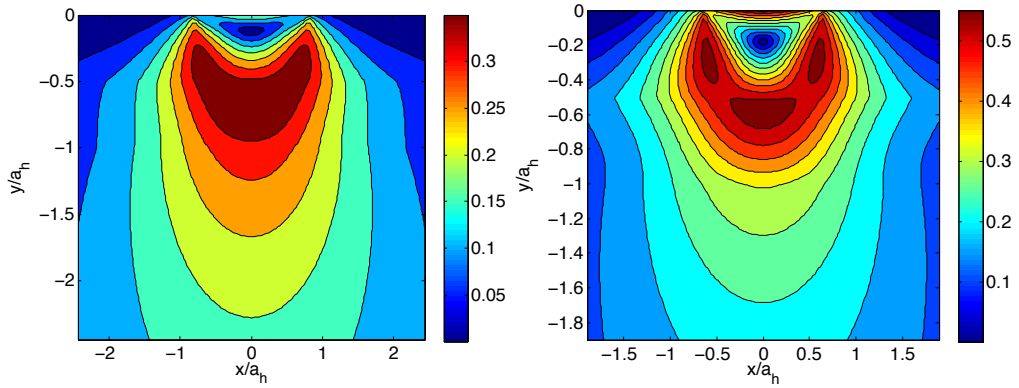

(c) $\mu_1/\mu_0 = 2$ (d) $\mu_1/\mu_0 = 4$

Figure 6: Plots of the dimensionless stress fields τ_1/P_{hertz} for the coatings given above. This set of results corresponds to the medium coating $h/a_h = 0.5$.

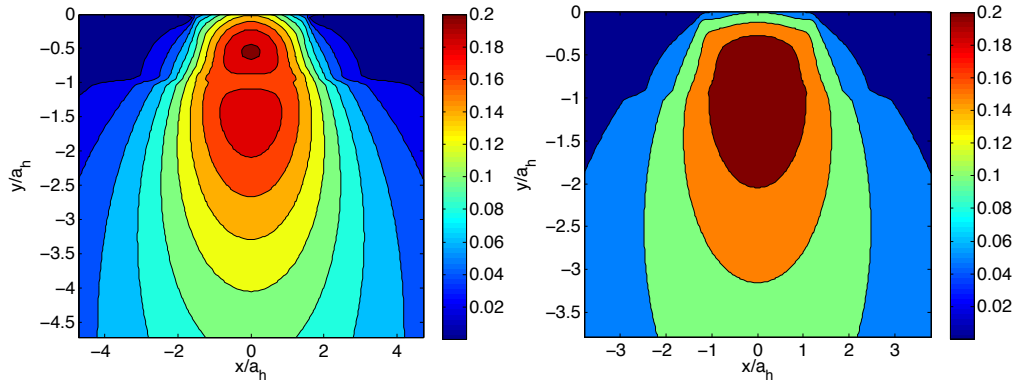

(a) $\mu_1/\mu_0 = 0.25$

(b) $\mu_1/\mu_0 = 0.5$

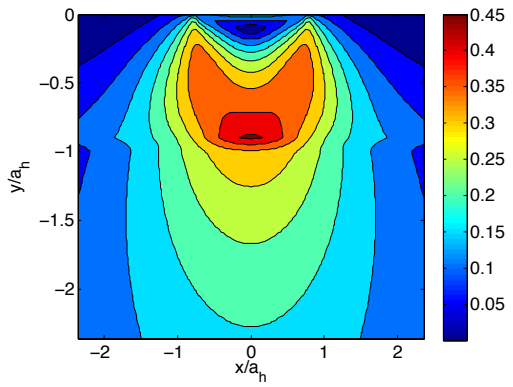

(c) $\mu_1/\mu_0 = 2$

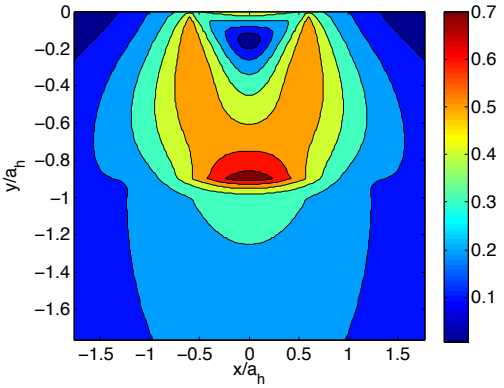

(d) $\mu_1/\mu_0 = 4$

Figure 7: Plots of the dimensionless stress fields τ_1/P_{hertz} for the coatings given above. This set of results corresponds to the thick coating $h/a_h = 0.9$.

$\frac{\mu_1}{\mu_0}$	quantity	$h_1/a_h = 0.1$	$h_1/a_h = 0.5$	$h_1/a_h = 0.9$
0.5	$\tau_{\max}/p_h$	0.25867877	0.24659909	0.24203556
	$y_{\max}/a_h$	-1.002	-1.074	-0.621
1	$\tau_{\max}/p_h$	0.30156241	0.30156272	0.30156291
	$y_{\max}/a_h$	-0.792	-0.792	-0.792
2	$\tau_{\max}/p_h$	0.36680373	0.39939964	0.45976487
	$y_{\max}/a_h$	-0.675	-0.675	-0.9

Table 1: The maximum principal stresses and the depth within the solid at which they occur for a range of coatings of different thickness.

as before and the ratio h_2/a_h is fixed within each problem so that only the coating thickness h_1 is allowed to vary. The dimensionless parameters a/a_h and $p_{\max}/p_h$ produced for three different layer thicknesses are plotted in figures (8) and (9). It is easily seen that the behaviour of the contact half-widths and maximum pressure become increasingly exaggerated as the interlayer becomes increasingly thin. We see that hard coatings experience much larger contact pressures as $h_2/h_2 \to 1$ whilst soft coatings experience much less pressure and thus we conclude that as $h_1/h_2 \to 1$, harder coatings will experience much larger maximum principal stresses whilst softer coatings will experience will smaller ones. The maximum principal stresses produced for a selection of different layer thicknesses and the position at which they occur are contained in table (1) and support this conclusion. It is interesting to note in this situation that the position of the maximum principal stress moves increasingly close to the interface $y = -h_2$ as $h_1/h_2 \to 1$ for harder coatings whilst it moves closer to the surface for softer coatings.

We conclude this example by investigating how the contact half-width and maximum pressure change with increasing load. It has already been observed that subject to a fixed load, the maximum contact pressure is larger for hard coatings but the contact region is larger for soft coatings and it is of interest to investigate if this trend continues as the load becomes increasingly large.

In this investigation, we cannot use a_h and p_h to non-dimensionalise the contact half-width and maximum pressure as these quantities are load dependent. We therefore consider the evolution of the parameters a/h_2 and $p_{\max}/\mu_0$ as the total dimensionless load $W/h_2\mu_0$ increases. The ratio $R/h_2 = 5$ is fixed in this problem whilst three different coating thicknesses are considered: $h_1/h_2 = 0.1, 0.5, 0.9$. The obtained contact half-widths and maximum contact pressures are presented in figure (10). We see that as the total load increases, the differences between the contact half-widths computed for hard and soft coatings and the maximum pressures become more marked. This is more noticeable as the ratio h_1/h_2 increases in and we therefore deduce that the values of a and $p_{\max}$ are more sensitive to the value of μ_1/μ_0 as the graded interlayer becomes thin.

7. Conclusions

We have derived a model which describes the horizontal and vertical displacements within an inhomogeneously elastic solid which comprises a homogeneously elastic coating and substrate joined together by a functionally graded transition layer. This model was then used to formulate an integral equation from which the contact pressure resulting from the rigid stamp problem can be determined. An iterative algorithm was then presented which further allows the contact half-width to be determined.

Two numerical examples that have previously been considered by other authors were re-examined

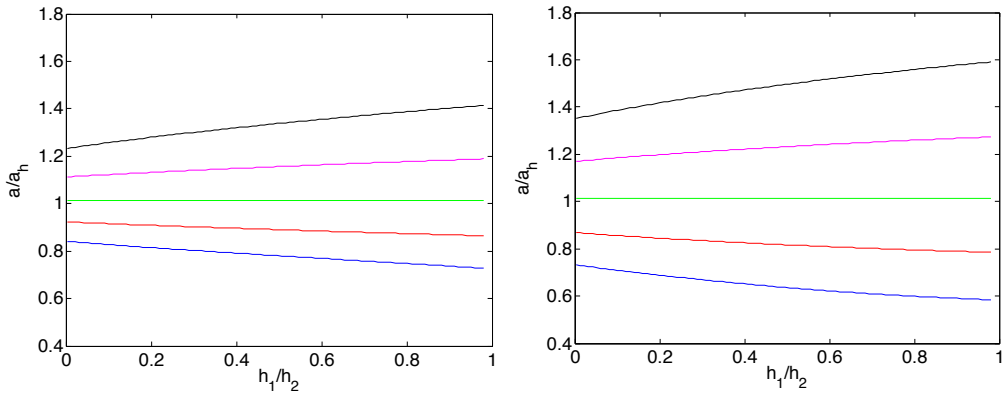

(a) $\frac{h_2}{a_h} = 0.1$ (b) $\frac{h_2}{a_h} = 0.5$

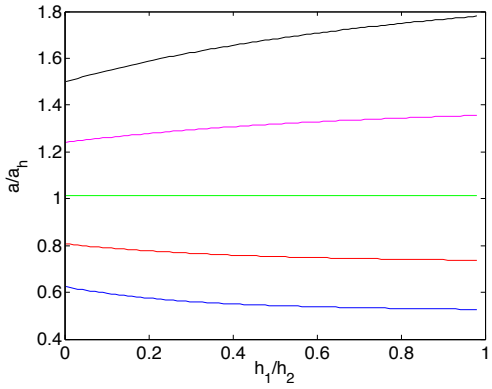

(c) $\frac{h_2}{a_h} = 0.9$

Figure 8: Plots of the evolution of the dimensionless contact half-width a/a_h for three different coating thicknesses. The blue line represents $\mu_1/\mu_0 = 4$, the red line $\mu_1/\mu_0 = 2$, the green line $\mu_1/\mu_0 = 1.00001$, the magenta line $\mu_1/\mu_0 = 0.5$ and the black line $\mu_1/\mu_0 = 0.25$.

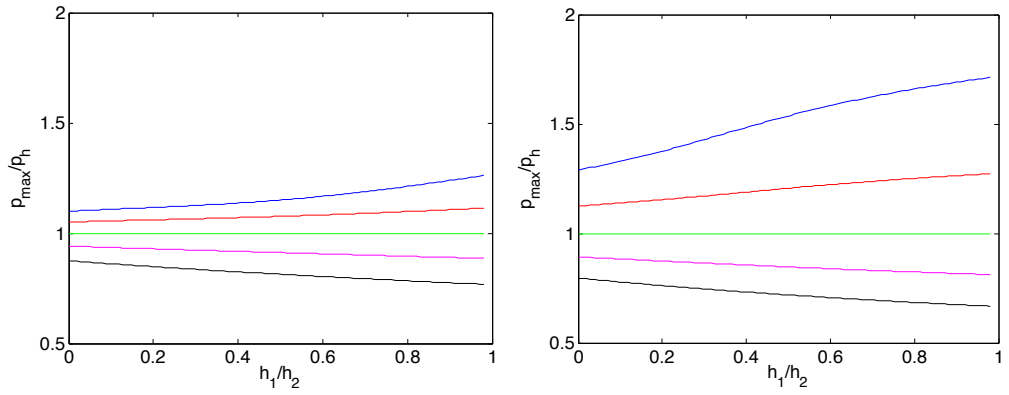

(a) $\frac{h_2}{a_h} = 0.1$ (b) $\frac{h_2}{a_h} = 0.5$

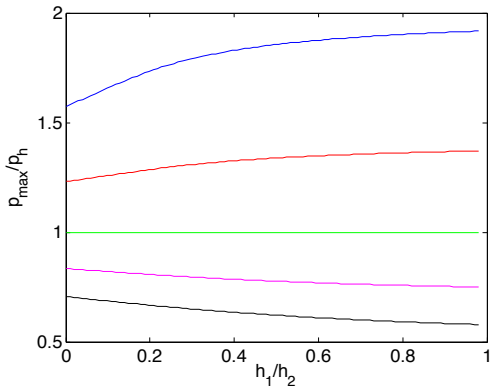

(c) $\frac{h_2}{a_h} = 0.9$

Figure 9: Plots of the evolution of the dimensionless maximum pressure $p_{\max}/p_h$ for three different coating thicknesses. The key is the same as that used in figure (8).

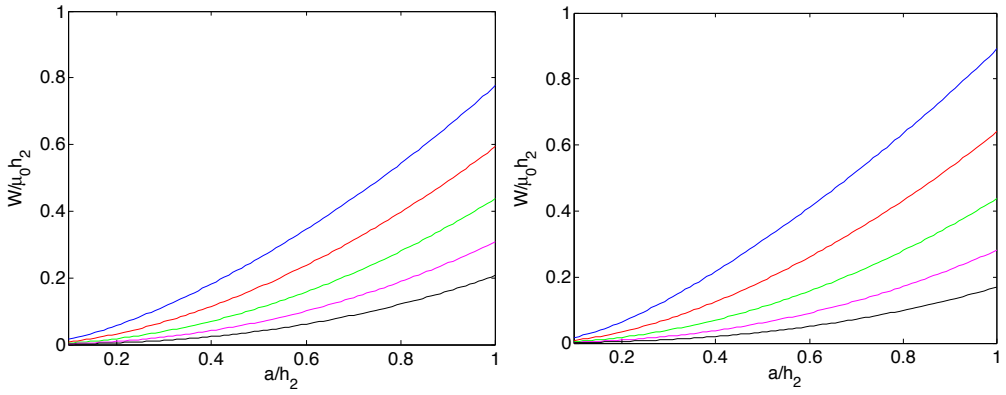

(a) $h_1/h_2 = 0.1$ (b) $h_1/h_2 = 0.5$

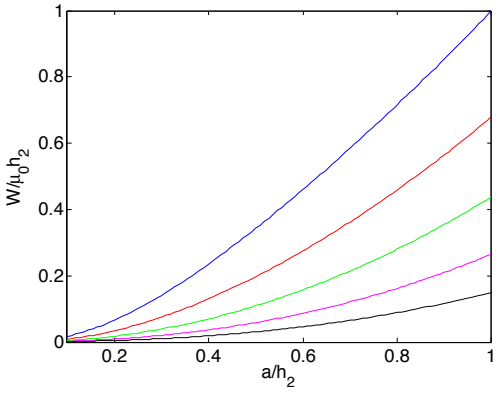

(c) $h_1/h_2 = 0.9$

Figure 10: Plots of the dimensionless contact half-width h_2/a against the dimensionless load for five different coatings.

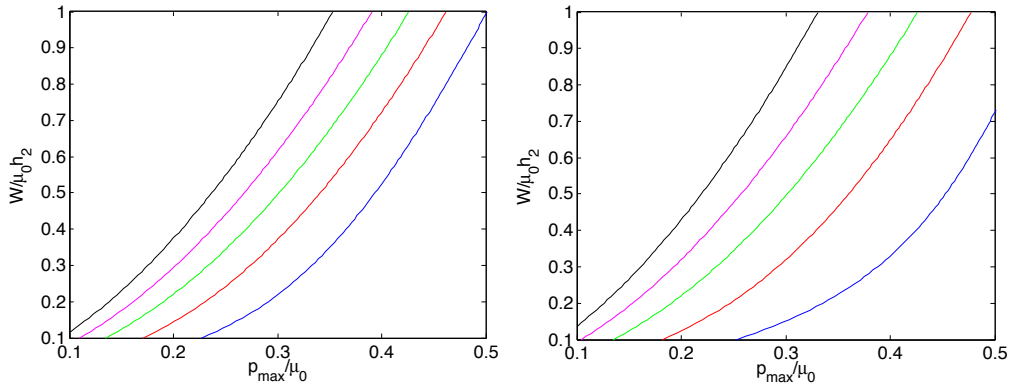

(a) $h_1/h_2 = 0.1$ (b) $h_1/h_2 = 0.5$

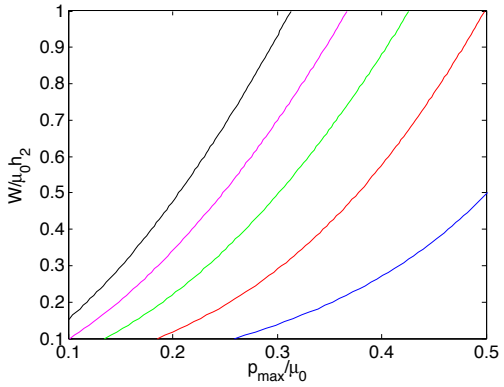

(c) $h_1/h_2 = 0.9$

Figure 11: Plots of the dimensionless maximum pressure $p_{\max}/\mu_0$ against the dimensionless load for five different coatings.

in this work and it was found that the solutions computed using our model are almost identical to those appearing in the original work. A further numerical example was presented that attempted to characterise the effects of varying coating and interlayer thickness as well as coating hardness on the solution of the contact problem. It was found that harder coatings experience pressures that have a larger maximum but act over a smaller region whilst softer coatings experience pressures with a smaller maximum that act over a larger area. This trend was found to be increasingly exaggerated as the interlayer thickness became negligible and indicates that the thickness of the graded elastic interlayer is directly responsible for changes in the maximum contact pressure and thus the maximum principal stress. This is very significant in determining material failure as small changes to the thickness of the coating and interlayer can lead to large differences in the resultant contact pressure.

Appendix A. Additional working for the full contact model

This section provides explicit expressions for the matrices appearing in section (3.2).

$$\Lambda_n = \begin{pmatrix} 2h_1+\delta_n & -2h_1^2 \\ 2 & \delta_n-2h_1 \end{pmatrix}, \tag{A.1}$$

$$J_n = \frac{1}{(3-4\nu)} \begin{pmatrix} 2(1-2\nu)(1-\nu)\beta_n & 2(1-\nu)(1-2\nu)\left(2(3-4\nu)-\beta_n h_1\right) \\ -4(1-\nu)\beta_n & 4(1-\nu)\beta_n h_1 \end{pmatrix}, \tag{A.2}$$

$$R_n = \begin{pmatrix} \frac{1}{2}\beta_n & -2(1-\nu) \\ \beta_n & -2(1-2\nu) \end{pmatrix}, \tag{A.3}$$

$$S_n = \begin{pmatrix} \frac{1}{2}\beta_n & 2(1-\nu) \\ -\beta_n & -2(1-2\nu) \end{pmatrix}, \tag{A.4}$$

$$Z^{(i)}_{j,n} = \begin{pmatrix} h_i(1+\gamma_{j,n})+\delta_n & h_i(1+\gamma_{j+2,n})+\delta_n \\ 1+\gamma_{j,n} & 1+\gamma_{j+2,n} \end{pmatrix}, \tag{A.5}$$

$$K^{(i)}_{j,n} = \begin{pmatrix} e^{-\lambda_{j,n}h_i} & 0 \\ 0 & e^{-\lambda_{j+2,n}h_i} \end{pmatrix}, \tag{A.6}$$

$$M_{j,n} = \begin{pmatrix} (1-2\nu)\left(1-2\nu-2(1-\nu)\gamma_{j,n}\right) & (1-2\nu)\left(1-2\nu-2(1-\nu)\gamma_{j+2,n}\right) \\ 2\left(2(1-\nu)-(1-2\nu)\gamma_{j,n}\right) & 2\left(2(1-\nu)-(1-2\nu)\gamma_{j+2,n}\right) \end{pmatrix}, \tag{A.7}$$

$$N_{j,n} = \begin{pmatrix} -\left((1-\nu)\gamma_{j,n}\lambda_{j,n}+\frac{1}{2}\nu\beta_n\right) & -\left((1-\nu)\gamma_{j+2,n}\lambda_{j+2,n}+\frac{1}{2}\nu\beta_n\right) \\ \lambda_{j,n}-\frac{1}{2}\beta_n\gamma_{j,n} & \lambda_{j+2,n}-\frac{1}{2}\beta_n\gamma_{j+2,n} \end{pmatrix}, \tag{A.8}$$

$$T_{j,n} = N_{j,n} - \frac{1}{\delta_n} M_{j,n}, \tag{A.9}$$

$$W_n = T_{1,n}K_{1,n}^{(1)} - T_{2,n}K_{2,n}^{(1)}(T_{2,n}K_{2,n}^{(2)})^{-1}T_{1,n}K_{1,n}^{(2)}, \tag{A.10}$$

$$\Phi_n = \frac{1}{\delta_n} R_n \left(Z_{1,n}^{(1)}K_{1,n}^{(1)} - Z_{2,n}^{(1)}K_{2,n}^{(1)}(T_{2,n}K_{2,n}^{(2)})^{-1}T_{1,n}K_{1,n}^{(2)} - \Lambda_n J_n^{-1} W_n \right) + e^{-\beta_n h_1} S_n J_n^{-1} W_n \tag{A.11}$$

for $i, j = 1, 2$.

Appendix B. Modelling an inhomogeneous solid comprising two homogeneous layers

The following work describes a mathematical model of the displacements u and v within an inhomogeneously elastic solid comprising two homogeneous yet distinct layers.

Using (17), (18), (25) and (26), we see that we may write the displacements within the coating as

$$u^{(1)}(x,y) = \sum_{n=1}^{\infty} \left(\left(C_n^{(1)} + C_n^{(2)} y \right) e^{\frac{1}{2}\beta_n y} + \left(C_n^{(3)} + C_n^{(4)} y \right) e^{-\frac{1}{2}\beta_n y} \right) \cos\left(\frac{1}{2}\beta_n (x+L) \right), \tag{B.1}$$

$$v^{(1)}(x,y) = \sum_{n=1}^{\infty} \left(\left(C_n^{(1)} + (y-\delta_n) C_n^{(2)} \right) e^{\frac{1}{2}\beta_n y} - \left(C_n^{(3)} + (y+\delta_n) C_n^{(4)} \right) e^{-\frac{1}{2}\beta_n y} \right) \sin\left(\frac{1}{2}\beta_n (x+L) \right), \tag{B.2}$$

which holds in the region $-L \leq x \leq L, -h_1 \leq y \leq 0$ and the displacements within the substrate as

$$u^{(2)}(x,y) = \sum_{n=1}^{\infty} \left(E_n^{(1)} + E_n^{(2)} y \right) e^{\frac{1}{2}\beta_n y} \cos\left(\frac{1}{2}\beta_n (x+L) \right), \tag{B.3}$$

$$v^{(2)}(x,y) = \sum_{n=1}^{\infty} \left(E_n^{(1)} + (y-\delta_n) E_n^{(2)} \right) e^{\frac{1}{2}\beta_n y} \sin\left(\frac{1}{2}\beta_n (x+L) \right) \tag{B.4}$$

which holds for $-L \leq x \leq L, -\infty < y < -h_1$.

We begin our attempt to solve for the constants within this problem by considering the interfacial matching conditions within this problem. These conditions which are applied at $y = -h_1$

are

$$u^{(1)} = u^{(2)}, \tag{B.5}$$

$$v^{(1)} = v^{(2)}, \tag{B.6}$$

$$\sigma_{yy}^{(1)} = \sigma_{yy}^{(2)}, \tag{B.7}$$

$$\sigma_{xy}^{(1)} = \sigma_{xy}^{(2)} \tag{B.8}$$

which ensure continuity of displacement and stress across the two layers. The conditions (B.5) and (B.6) yield the system

$$e^{-\frac{1}{2}\beta_n h_1} G_n \begin{pmatrix} C_n^{(1)} \\ C_n^{(2)} \end{pmatrix} + e^{\frac{1}{2}\beta_n h_1} H_n \begin{pmatrix} C_n^{(3)} \\ C_n^{(4)} \end{pmatrix} = e^{-\frac{1}{2}\beta_n h_1} G_n \begin{pmatrix} E_n^{(1)} \\ E_n^{(2)} \end{pmatrix} \tag{B.9}$$

where the matrices G_n and H_n are defined as

$$G_n = \begin{pmatrix} 1 & -h_1 \\ 1 & -(h_1 + \delta_n) \end{pmatrix}, \tag{B.10}$$

$$H_n = \begin{pmatrix} 1 & -h_1 \\ -1 & h_1 - \delta_n \end{pmatrix}. \tag{B.11}$$

Equations (B.7) and (B.8) similarly reveal the system

$$\frac{\mu_1}{\mu_0} \left(e^{-\frac{1}{2}\beta_n h_1} R_n^{(1)} \begin{pmatrix} C_n^{(1)} \\ C_n^{(2)} \end{pmatrix} + e^{\frac{1}{2}\beta_n h_1} S_n^{(1)} \begin{pmatrix} C_n^{(3)} \\ C_n^{(4)} \end{pmatrix} \right) = e^{-\frac{1}{2}\beta_n h_1} R_n^{(1)} \begin{pmatrix} E_n^{(1)} \\ E_n^{(2)} \end{pmatrix}. \tag{B.12}$$

Finally the surface boundary conditions applied within this problem are the same as those used in the full three-layer model, so that we obtain the final system

$$R_n^{(0)} \begin{pmatrix} C_n^{(1)} \\ C_n^{(2)} \end{pmatrix} + S_n^{(0)} \begin{pmatrix} C_n^{(3)} \\ C_n^{(4)} \end{pmatrix} = -\frac{1}{2\mu_1} \begin{pmatrix} P_n \\ 0 \end{pmatrix}. \tag{B.13}$$

The matrices $R_n^{(i)}$ and $S_n^{(i)}$, $i = 0, 1$ are defined as

$$R_n^{(i)} = \begin{pmatrix} \frac{1}{2}\beta_n & -\left(\frac{1}{2}\beta_n h_i + 2(1-\nu)\right) \\ \beta_n & -(2(1-2\nu)+\beta_n h_i) \end{pmatrix} \tag{B.14}$$

with $y = -h_0 = 0$ for notational convenience. We can combine (B.10), (B.12) and (B.13) to obtain the results

$$\begin{pmatrix} C_n^{(1)} \\ C_n^{(2)} \end{pmatrix} = -\frac{1}{2\mu_1}\Phi_n^{-1} \begin{pmatrix} P_n \\ 0 \end{pmatrix}, \tag{B.15}$$

$$\begin{pmatrix} C_n^{(3)} \\ C_n^{(4)} \end{pmatrix} = e^{-\beta_n h_1}\left(1-\frac{\mu_1}{\mu_0}\right)\left(\frac{\mu_1}{\mu_0}S_n^{(1)} - R_n^{(1)}G_n^{-1}H_n\right)^{-1} R_n^{(1)} \begin{pmatrix} C_n^{(1)} \\ C_n^{(2)} \end{pmatrix}, \tag{B.16}$$

$$\begin{pmatrix} E_n^{(1)} \\ E_n^{(2)} \end{pmatrix} = \begin{pmatrix} C_n^{(1)} \\ C_n^{(2)} \end{pmatrix} + e^{\beta_n h_1} G_n^{-1} H_n \begin{pmatrix} C_n^{(3)} \\ C_n^{(4)} \end{pmatrix} \tag{B.17}$$

with

$$\Phi_n = R_n^0 + e^{-\beta_n h_1}\left(1-\frac{\mu_1}{\mu_0}\right) S_n^{(0)} \left(\frac{\mu_1}{\mu_0}S_n^{(1)} - R_n^{(1)}G_n^{-1}H_n\right)^{-1} R_n^{(1)}. \tag{B.18}$$

If we multiply the matrices appearing in this expression together, we find that

$$R_n^{(1)}G_n^{-1}H_n = \frac{1}{\delta_n}\begin{pmatrix} -1 & h_1 - 2(1-nu)\delta_n \\ 2 & -2\left((1-2\nu)\delta_n + h_1\right) \end{pmatrix},$$

$$\frac{\mu_1}{\mu_0}S_n^{(1)} - R_n^{(1)}G_n^{-1}H_n = \frac{1}{\delta_n}\begin{pmatrix} (3-4\nu)\frac{\mu_1}{\mu_0}+1 & 2(1-\nu)\delta_n\left(1+\frac{\mu_1}{\mu_0}\right) - h_1\left(1+(3-4\nu)\frac{\mu_1}{\mu_0}\right) \\ -2\left((3-4\nu)\frac{\mu_1}{\mu_0}+1\right) & 2\left(h_1\left(1+(3-4\nu)\frac{\mu_1}{\mu_0}\right) + (1-2\nu)\delta_n\left(1-\frac{\mu_1}{\mu_0}\right)\right) \end{pmatrix}$$

and thus

$$\left(1-\frac{\mu_1}{\mu_0}\right)\left(\frac{\mu_1}{\mu_0}S_n^{(1)}-R_n^{(1)}G_n^{-1}H_n\right)^{-1}R_n^{(1)}=\frac{\left(\frac{\mu_0}{\mu_1}-1\right)\beta_n}{2\left((3-4\nu)+\frac{\mu_0}{\mu_1}\right)\left((3-4\nu)\frac{\mu_0}{\mu_1}+1\right)}\times$$
$$\begin{pmatrix}(2h_1-\delta_n)\left((3-4\nu)+\frac{\mu_0}{\mu_1}\right) & -\frac{2}{\beta_n}\left(h_1^2\beta_n\frac{\mu_0}{\mu_1}+(3-4\nu)\beta_n h_1^2-4(1-2\nu)(1-\nu)\delta_n\right)\\ 2\left((3-4\nu)+\frac{\mu_0}{\mu_1}\right) & -(2h_1+\delta_n)\left(\frac{\mu_0}{\mu_1}+(3-4\nu)\right)\end{pmatrix}. \tag{B.19}$$

Acknowledgement

The authors acknowledge the technical support from partners and sponsorship provided by the EPSRC through the ENCYCLOPAEDIC program grant.

References

, .

Chidlow, S.J., Teodorescu, M., Vaughan, N.D., 2011. Predicting the deflection and sub-surface stress field within two-dimensional inhomogeneously elastic bonded layered solids under pressure. Int. J. Solids Structures 48, 3243–3256.

Guler, M.A., Erdogan, F., 2004. Contact mechanics of graded coatings. Int. J. Solids Structures 41, 3865–3889.

Guler, M.A., Erdogan, F., 2007. The frictional sliding contact problems of rigid parabolic and cylindrical stamps on graded coatings. Int. J. Mech. Sci. 49, 161–182.

Hannah, M., 1951. Contact stress determination in a thin elastic layer. Q. J. Mech. Appl. Math. 4, 94–105.

Jaffar, M.J., 1989. Asymptotic behaviour of thin elastic layers bonded and unbonded to a rigid foundation. Int. J. Mech. Sci 31, 229–235.

Ke, L.L., Wang, Y.S., 2006. Two-dimensional contact mechanics of functionally graded materials with arbitrary spatial variations of material properties. Int. J. Solids Structures 43, 5779–5798.

Ke, L.L., Wang, Y.S., 2007. Two-dimensional sliding frictional contact of functionally graded materials. European Journal of Mechanics A/Solids 26, 171–188.

Ma, L.F., Korsunsky, A.M., 2004. Fundamental formulation for frictional contact problems of coated systems. Int. J. Solids Structures 41, 2837–2854.

Porter, D., Stirling, D.S.G., 1990. Integral equations. Cambridge University Press, Cambridge.

Teodorescu, M., Rahnejat, H., Gohar, R., Dowson, D., 2009. Harmonic decomposition analysis of contact mechanics of bonded layered elastic solids. Applied Mathematical Modelling 33, 467–485.

Yang, J., Ke, L.L., 2008. Two-dimensional contact problem for a coating-graded layer-substrate structure under a rigid cylindrical punch. Int. J. Mech Sciences 50, 985–994.